nature physics

ARTICLES

https://doi.org/10.1038/s41567-020-01123-w

Check for updates

Exchange bias due to coupling between coexisting antiferromagnetic and spin-glass orders

Eran Maniv[1,2]✉, Ryan A. Murphy[3], Shannon C. Haley[1,2], Spencer Doyle[1,2], Caolan John[1,2], Ariel Maniv[4,5], Sanath K. Ramakrishna[5], Yun-Long Tang[1,2,6], Peter Ercius[7], Ramamoorthy Ramesh[1,2,6], Arneil P. Reyes[5], Jeffrey R. Long[2,3,8] and James G. Analytis[1,2]✉

Exchange bias is a property of widespread technological utility, but its underlying mechanism remains elusive, in part because it is rooted in the interaction of coexisting order parameters in the presence of complex magnetic disorder. Here we show that a giant exchange bias housed within a spin-glass phase arises in a disordered antiferromagnet. The magnitude and robustness of the exchange bias emerges from a convolution of two energetic landscapes, namely the highly degenerate landscape of the spin glass biased by the sublattice spin configuration of the antiferromagnet. The former provides a source of uncompensated moment, whereas the latter provides a mechanism for its pinning, which leads to the exchange bias. Tuning the relative strengths of the spin-glass and antiferromagnetic order parameters reveals a principle for tailoring the exchange bias, with potential applications to spintronic technologies.

Technologies that rely on the correlated properties of quantum materials are one of the most active areas of research at the boundary of physics and engineering. One such property is exchange bias. It is an important mechanism in a variety of devices such as spin valves, is used extensively in high-density magnetic storage[1], and has potentially more exotic applications including voltage-mediated magnetic switching for logic devices[2]. Exchange bias manifests itself as a shift in the hysteresis loop of a magnetic system when the system is cooled under an applied external field[3], and is observed in a number of different systems. Despite decades of study of the prototypical exchange bias system, thin-film ferromagnet/antiferromagnet (FM/AFM) heterostructures, a complete understanding of the mechanism behind exchange bias is lacking. Recent work has revealed that pinned uncompensated moments that are generated by defects at the FM/AFM interface play a dominant role in engendering exchange bias, as well as in determining its magnitude[4–6]. The microscopic nature of the pinned uncompensated moment interface, how it is pinned by the antiferromagnetic order parameter, and the mechanism by which this coupling drives exchange bias remain outstanding challenges. Importantly, this interface may host its own 'hidden' glassy order parameter, driven by spin frustration from disorder at the FM/AFM interface itself. Indeed, spin glasses alone may display exchange bias, and this in concert with studies on ferromagnetic/spin-glass interfaces have led to hypotheses that suggest that glassy dynamics are intertwined with exchange bias[7–11].

Spin glasses are a phase of matter that occurs in many strongly correlated systems, but differ from ordered FMs or AFMs in that their ground state is metastable, as one of many nearly degenerate states[12,13]. Frustration, which emerges as a result of site disorder[14,15] or local competition between exchange interactions[16], is of central importance in these systems. The frustration protects the ergodicity of the system until it reaches the spin-glass transition, at which point a metastable state is settled upon. Understanding the dynamic processes by which the glass traverses through this energetic landscape remains a major theoretical question in the statistical mechanics of solids. Theoretical challenges notwithstanding, the frozen state of the spin glass depends on its history, in particular the applied field in which it was cooled. This is the origin of its exchange bias; the magnetism of the frozen state is biased by the correlations of the spin glass. Typically this bias is very small, of the order of 0.01 T.

In this work, we use the highly field-responsive nature of the spin-glass order parameter as a source of pinned uncompensated moment, and embed this within an anisotropic AFM. By isolating these phases in the absence of a FM, we are explicitly able to study the exchange coupling between the antiferromagnetic order parameter (defined as the stability of the sublattice magnetization) and the spin-glass order parameter (defined as the breaking of ergodicity of fluctuating, disordered spins[17]). Using the material Fe_xNbS_2 as an example, we show that when the uncompensated moments form a spin glass, giant lateral shifts in the hysteresis loops appear. We find that the antiferromagnetic order parameter biases the response of the spin glass, but only when both become long-time correlated. The origin of the exchange bias therefore lies in the convolution of two energy landscapes, namely the highly degenerate landscape of the spin glass biased by the sublattice phase space of the AFM. Furthermore, our intercalation series enables us to tune the relative stability of both spin-glass and antiferromagnetic order parameters by changing the composition x, thereby outlining a route towards the development of new giant exchange bias phases.

Fe_xNbS_2 consists of triangular lattices of iron embedded between 2H-NbS_2 layers. Single crystals were synthesized by using conventional vapour transport techniques while varying concentrations of iron (see Supplementary Sections 1–6 for characterization of

[1]Department of Physics, University of California, Berkeley, CA, USA. [2]Materials Sciences Division, Lawrence Berkeley National Laboratory, Berkeley, CA, USA. [3]Department of Chemistry, University of California, Berkeley, CA, USA. [4]Nuclear Research Center – Negev, Beer Sheva, Israel. [5]National High Magnetic Field Laboratory, Tallahassee, FL, USA. [6]Department of Materials Science and Engineering, University of California, Berkeley, CA, USA. [7]National Center for Electron Microscopy, Molecular Foundry, Lawrence Berkeley National Laboratory, Berkeley, CA, USA. [8]Department of Chemical and Biomolecular Engineering, University of California, Berkeley, CA, USA. ✉e-mail: eranmaniv@berkeley.edu; analytis@berkeley.edu

homogeneity and stoichiometry). This material manifests antiferromagnetic hexagonal ordering[18–20] with the moment predominantly oriented along the c axis. For intercalation values less than $x = \frac{1}{3}$, spin-glass-like behaviour has been observed in magnetization and heat capacity measurements[21–23]. Magnetization versus temperature measurements that were performed along the c axis on Fe_xNbS_2 for under-intercalated ($x = 0.30$) and over-intercalated ($x = 0.35$) values are shown (Fig. 1a,c). For $x \approx \frac{1}{3}$, which corresponds to the fully packed $Fe_{1/3}NbS_2$ structure, we observe a sharp antiferromagnetic transition with a Néel temperature, T_N, of approximately 42 K (Supplementary Section 14), as has been previously reported[20,22,24–26]. Above or below $x = \frac{1}{3}$, field-cooled and zero-field-cooled curves begin to separate, which indicates the presence of a frozen moment. The magnetization is observed to relax with time on removal of the applied field for such compositions, which is characteristic of spin glass behaviour (Fig. 1b,d) (ref. [13]). The temperature onset of long relaxation times arises from the formation of an uncompensated moment that is observed when field-cooled and zero-field-cooled curves separate substantially. This temperature is roughly where the spin glass freezes on the time scale of the measurement and the ergodicity of the system is broken; the spin configuration of the uncompensated moment is long-time correlated. Further experiments corroborate the glass state (as detailed in Supplementary Sections 6, 9, 10 and 12).

The disorder opens up a hysteresis loop whose centre strongly depends on the cooling field. We illustrate the low-temperature hysteresis loop for samples cooled in 7 T and then field-cycled across ±7 T ten times (Fig. 2a,c). This 'training' of the hysteresis loop is consistent with exchange bias, and shows that the loop centre becomes pinned at large fields, approximately 3 T for $x = 0.30$ and 0.7 T for $x = 0.35$ (refs.[13,27]). We show enlargement of zero-field-cooled hysteresis loops (Fig. 2b,d), but with two different protocols for the field sweeps. For sweeps starting negative ($0 \rightarrow -7 \rightarrow +7 \rightarrow -7$), the loop centre shifts to positive field; for sweeps starting positive ($0 \rightarrow +7 \rightarrow -7 \rightarrow +7$), the loop centre moves to negative field. This spontaneous bias points to a history-dependent coupling scheme between the antiferromagnetic and spin-glass phases that is substantially more sensitive than in typical exchange bias systems.

The temperature-dependent evolution of H_{EB} (defined as the average of the zero-magnetization intercepts) and H_C (defined as the half-width of the hysteresis loop at the average of the zero-field intercepts) presents a non-trivial dependence (Fig. 3a,c). The onset of H_C occurs at around the spin glass freezing temperature as expected, whereas the onset of bias H_{EB} occurs at a substantially lower temperature. The reason for this can be gleaned from measurements of nuclear magnetic resonance (NMR) spectra (Fig. 4). The iron exchange field is studied via its effect on the ^{93}Nb lattice (with nuclear spin $I = 9/2$ and gyromagnetic ratio $\gamma = 10.405\,\mathrm{MHz\,T^{-1}}$). In the paramagnetic state at temperatures $T > T_N$, the spectra exhibit a broad peak with quadrupolar splitting originating from two Nb unit cell sites. Below T_N the system splits into a double-peak structure around the paramagnetic centre. This is a signature of antiferromagnetic order, with the two peaks originating from the two sublattices where the local hyperfine field (approximately 1 T) adds to, and subtracts from, the externally applied magnetic field[28]. The peak structure onset is substantially below T_N, which suggests that it is only at these temperatures that the antiferromagnetic order parameter is well formed. These lower temperatures correspond to the onset of H_{EB} (Fig. 3a), which is a direct validation of the hypothesis that the exchange bias arises from the coexistence of the antiferromagnetic order parameter with the spin glass. It is also notable that the peaks of dilute and excess intercalations are asymmetric (Fig. 4a,c), in contrast to the stoichiometric case (Fig. 4b), which suggests that coupling between the spin glass and the AFM exerts an internal exchange field on the ^{93}Nb lattice: spin-glass-pinned uncompensated moments align with one antiferromagnetic sublattice. This provides direct evidence for the existence of exchange coupling between the spin-glass and the antiferromagnetic order parameters.

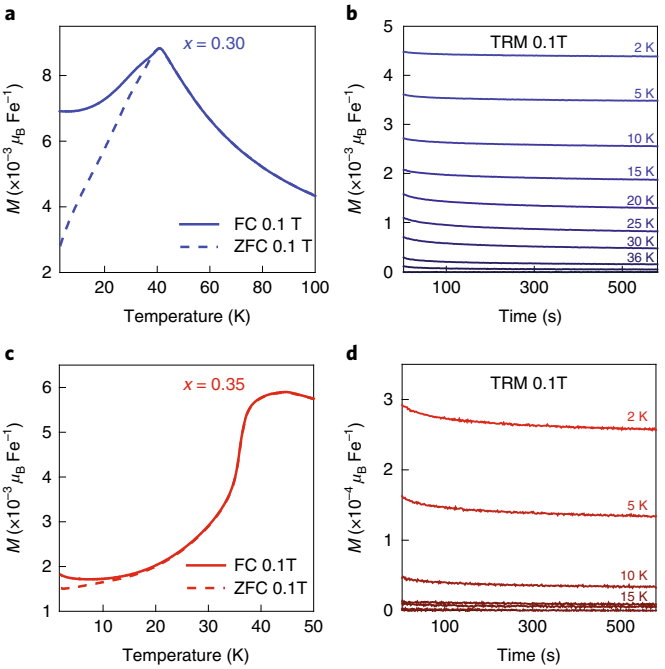

Fig. 1 | Spin glass characterization of Fe_xNbS_2 for $x = 0.30$ and $x = 0.35$. **a**,**c**, Magnetization versus temperature for each intercalation value measured in a field of 0.1 T; both the field-cooled (FC, solid line) and zero-field-cooled (ZFC, dashed line) curves are shown. The samples were field-cooled in a field of 0.1 T. The antiferromagnetic transition temperature (T_N) correlates to the sharp drop in magnetization (approximately 41 K for $x = 0.30$ (**a**) and 37 K for $x = 0.35$ (**c**)). The divergence of the FC and ZFC curves demonstrates the onset of a glassy frozen moment, which we identify as the effective spin glass freezing temperature (approximately 38 K for $x = 0.30$ and 15 K for $x = 0.35$). From Curie–Weiss fits, we extract effective moments of 5.4, 5.2 and 5.4 μ_B Fe^{-1} (where μ_B is the Bohr magneton) for $x = 0.30$, 0.31 and 0.35 intercalations, respectively (for full data and analysis, see Supplementary Section 8). **b**,**d**, Thermoremanent magnetization (TRM) measurements performed at various temperatures after the samples were field-cooled in a field of 0.1 T. The relaxations were measured after the magnetic field was removed. The y axis exhibits an order of magnitude difference between $x = 0.30$ (**b**) and $x = 0.35$ (**d**) intercalations. The appearance of relaxation dynamics is correlated with the glassy state. Additional isothermal remanent magnetization measurements, performed after the samples were zero-field-cooled, present similar dynamics, which indicates a common relaxation mechanism in both routines (see Supplementary Section 9 for full analysis).

Although the low-field hysteresis loop is opened by the presence of disorder, the coupling to the antiferromagnetic order parameter means that it cannot close independently of the AFM. This motivates us to study the exchange bias at magnetic fields that are high enough to drive a metamagnetic transition in the AFM[20]. It has been recently shown that the antiferromagnetic order of the stoichiometric compound undergoes a metamagnetic transition from a stripe to an up-up-up-down phase at $H_{plat} \approx 17$ T, which is characterized by a plateau in the magnetization[20]. This same transition is observed at all compositions, albeit greatly broadened by disorder owing to the deviation from $x = \frac{1}{3}$. Hysteresis loops close only at fields that go well beyond the metamagnetic transition for any composition (Fig. 5); the hysteretic response of the spin glass is coupled to the magnetic

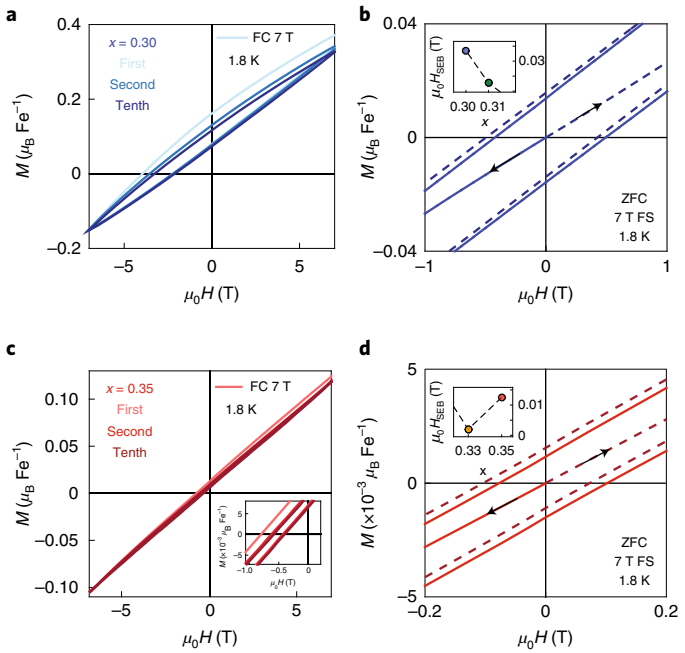

Fig. 2 | Low-field exchange bias characterization. a,**c**, Shifted magnetic hysteresis loops measured after the samples are cooled from above the transition temperature ($x = 0.30$ (**a**) and $x = 0.35$ (**c**)). The slight decrease of the shifted hysteresis loops and their coercivity after ten consecutive field sweeps demonstrates a training process in which the exchange bias is robust (see inset for $x = 0.35$ intercalation). **b**,**d**, Zoom-in on hysteresis loops taken at 1.8 K after cool-down without any external field ($x = 0.30$ (**b**) and $x = 0.35$ (**d**)). For each intercalation the magnetic field sweep (FS) was performed twice, with the sweep started in the negative direction (solid lines) or in the positive direction (dashed lines). A spontaneous exchange bias of a few hundred Oersted, which is dependent on the initial sweep direction, is visible. The insets show the monotonic increase in the spontaneous exchange bias field, H_{SEB}, when departing from the $x = \frac{1}{3}$ intercalation.

response of the AFM. Importantly, saturating the magnetization at these high fields also ensures that the sample is in the metamagnetic major loop. In conjunction with the spontaneous bias observed at both low and high fields (an effect incompatible with minor loops), these data show that the observed exchange bias cannot be attributed to minor loop effects. Low-field cooled loops are less easy to disentangle from minor loop phenomena, but their robust bias after multiple training loops is also inconsistent with minor loops (see extended discussion in Supplementary Section 11).

To see the effects of the field-cooled history, we study H_{EB} and H_C when the system is cooled in a field H_{FS} and then cycled across $\pm H_{FS}$. H_C tends to increase with higher H_{FS} for all compositions (Fig. 3d), which suggests that the exchange anisotropy of the spin glass grows as the field in which it was cooled increases, as in typical glassy systems. H_{EB}, however, is more directly correlated with the response of the antiferromagnetic order. The peak exchange bias of the $x = 0.30$ sample exceeds $H_{EB} \approx 3$ T at relatively low fields, followed by a monotonic decrease at fields beyond H_{plat}, until no memory of magnetization history remains and $H_{EB} \to 0$ (Fig. 3b). The $x = 0.31$ sample follows a similar trend but subsequently plateaus at high fields, which suggests a marginally more robust exchange bias (Fig. 3b). For $x = 0.35$, H_{EB} shows a kink at the metamagnetic transition, but interestingly it saturates at high fields to $H_{EB} \approx 1$ T, which is substantially higher than that of the diluted systems (Fig. 3b). For an exchange bias, this is orders of magnitude greater than that observed in typical heterostructure or spin-glass systems[13], but is actually much closer to many theoretically predicted values in the absence of disorder[29]. The large bias is housed within the uncompensated moments of the spin glass, pinned by the coexisting AFM.

Our data suggest that the bias can be understood by considering the interplay of energy landscapes between the spin glass and the AFM, as well as their exchange coupling. In the Sherrington–Kirkpatrick model, each possible state in an ergodic landscape of possible spin configurations is roughly interchangeable when looked at through the lens of spatial spin fluctuations. Above the spin-glass transition, the accessible states are energetically equivalent. Below the spin-glass transition, this ergodicity is broken by the freezing of the random spin texture[17]. However, the other possible states are only weakly distinguished in energy, so that effects such as exchange bias, which rely on restricting the accessible phase space volume, are generally small (of the order of 0.01 T). By contrast, in an easy-axis AFM only one of two degenerate states, corresponding to distinct spin orientations, is possible for a local spin. Indeed, experiments on the present system with an in-plane field $H \| ab$,

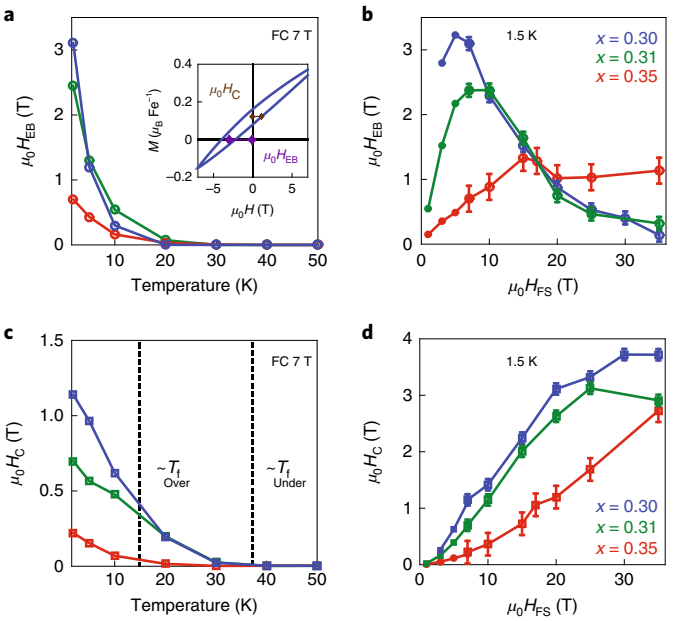

Fig. 3 | Temperature and field sweep dependencies of the exchange bias and coercive fields. a,**c**, Temperature dependence of the extracted exchange bias (**a**) and coercive fields (**c**) for $x = 0.30$, 0.31 and 0.35 intercalations, after cooling in a 7 T magnetic field from above the antiferromagnetic transition. For the inset in **a**, the exchange bias field, H_{EB} (purple), was extracted from each loop by taking the average of the x intercepts, $H_{EB} = \frac{H_{int1}+H_{int2}}{2}$; the coercive field, H_C (brown), was calculated from the half-width of the hysteresis loop at the average of the y intercepts. The dashed lines **c** mark the approximate spin glass freezing temperature (T_f) for under(over)-intercalated samples, according to the FC/ZFC divergence presented in Fig. 1a,c. **b**,**d**, The extracted exchange bias (**b**) and coercive fields (**d**) versus the sweeping field, H_{FS}, for $x = 0.30$, 0.31 and 0.35 intercalations, measured at 1.5 K. The $x = 0.30$ intercalation was cooled in a 7 T magnetic field. For $x = 0.31$ and 0.35 intercalations, the cooling fields are identical to the field sweep range. H_{EB} shows a non-monotonic response as the swept field passes through the metamagnetic transition. For under-intercalated samples the exchange bias at high fields is suppressed, vanishing for $x = 0.30$ intercalation and saturating (around 0.3 T) for $x = 0.31$. Conversely, for over-intercalation ($x = 0.35$) the high field exchange bias is saturated around 1 T. H_C grows monotonically with no distinct variation in the field range of the metamagnetic transition. The error bars are defined by the x (H_{EB}) and y (H_C) intercepts resolution.

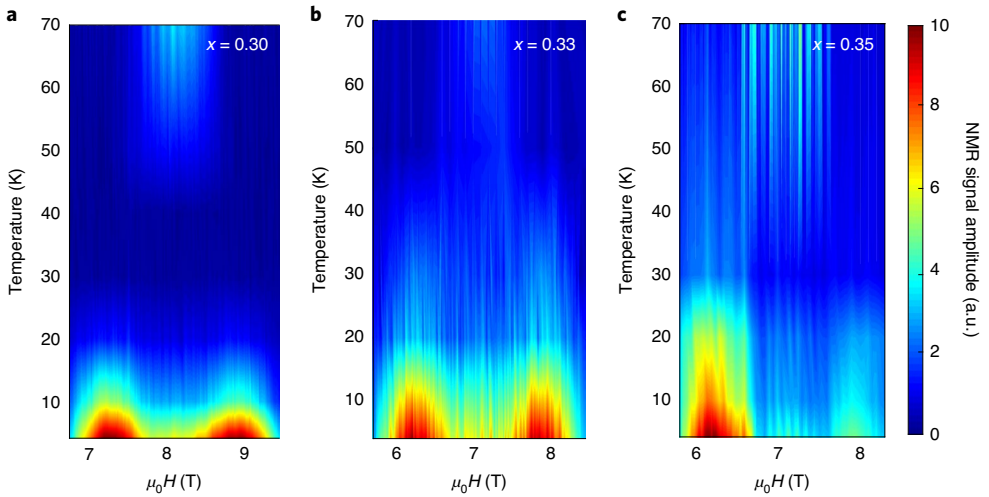

Fig. 4 | NMR measurements performed on $x = 0.30$, 0.33 and 0.35 intercalations. a–c, Field-swept NMR spectra at 85 MHz ($x = 0.30$) and 74.5 MHz ($x = 0.33$ and 0.35) measured at several temperatures between 70 K and 4.2 K. The samples were cooled and measured in a magnetic field oriented along the *c* axis. For $x = 0.30$ intercalation, the 4.2 K field sweep was zero-field-cooled. The colour maps of the NMR amplitude (normalized and scaled by their maximum value) are interpolations of the raw data. All samples show a single paramagnetic quadrupolar spectrum at high temperatures that splits into two broad peaks at low temperatures owing to antiferromagnetic ordering. **a**, As the temperature is lowered, the Nb peaks broaden for the $x = 0.30$ sample. At temperatures below 20 K, two broad peaks indicative of a long-range antiferromagnetic order emerge. In addition, an asymmetry component between the two peaks is present. **b**, The stoichiometric sample ($x = 0.33$) shows a similar peak structure but with no asymmetry. For this intercalation, the antiferromagnetic phase is not affected by cooling in a magnetic field. **c**, For the $x = 0.35$ sample, the Nb peaks are clearly visible at all temperatures, which indicates that the iron lattice is highly ordered. Below 25 K, two broad peaks with a massive asymmetry component appear.

reveal substantially smaller H_{EB}, on the order of a typical spin-glass exchange bias (Supplementary Section 13), which confirms that the phase space of in-plane configurations is unaffected by the coexisting AFM. However, our measurements of giant exchange bias in the interlayer direction suggest that the coexistence of an AFM biases the glassy landscape, strongly distinguishing the possible spin states in energy by leveraging the sublattice broken symmetry of the AFM. This is the origin of the bias; in changing the landscape of the spin glass, the uncompensated moment becomes pinned by the coexisting texture of the AFM.

Our intercalation series further enables us to uniquely describe the roles that glassy disorder and antiferromagnetic anisotropy play in exchange bias systems. A comparison of the relaxation dynamics indicates that the glass phase is more polarizable, is thermally persistent, and relaxes more slowly as iron concentration decreases from over-intercalated to under-intercalated samples (Fig. 1b,d and Supplementary Sections 9 and 10). This trend follows the trend of the maximum amplitude of the exchange bias field; below the metamagnetic transition, the glassier samples are more responsive to their field history, which results in a correspondingly larger exchange bias amplitude (Fig. 3b). Above the metamagnetic transition, the relative stability of the antiferromagnetic order parameter determines the robustness of the bias. We show data from samples field-cooled at H_{FC} but swept beyond $\pm H_{plat}$ (Fig. 5). This way, the effect of the field-cooled history of the spin glass can be separated from the effects of sweeping across the metamagnetic transition. As shown, in every case H_{EB} saturates at a single value at any field that exceeds H_{plat}, approaching 0 T, 0.3 T and 1 T for $x = 0.30$, 0.31 and 0.35 respectively. (Note that the figure shows examples of both 30 T and 35 T field sweeps, which are both greater than H_{plat}.) These values are the same asymptotic values approached at high field (Fig. 3b), which suggests that the exchange bias of the spin glass depends on the ground state of the AFM.

The resilient, larger exchange bias that results from over-intercalation can be understood by considering its local structure. In the under-intercalated samples, vacancies are introduced in the antiferromagnetic lattice, whereas in the over-intercalated sample the glass component instead sits on interstitial positions throughout the fully packed antiferromagnetic structure. As the antiferromagnetic component of the over-intercalated sample is fully intact, the anisotropy of the AFM and its ability to strongly bias the spin glass is retained even at high fields, which results in a substantially larger exchange bias of approximately 1 T in comparison to the exchange bias plateau observed in the $x = 0.31$ system. NMR experiments support a more robust AFM in over-intercalated samples; the antiferromagnetic order parameter appears at higher temperatures and with more intact fine structure than in the under-intercalated sample. This is further evidenced by heat capacity profiles, as under-intercalated samples are featureless whereas the over-intercalated sample displays a broad peak (see further discussion in Supplementary Section 6). The nature of the defects determines how easily they can be pinned and therefore the maximum bias value to the spin glass, but the robustness of the AFM determines the degree of this pinning and therefore whether the exchange bias can be maintained at high magnetic fields. This division of labour demonstrates a unique strategy that is broadly applicable in the design of new giant exchange bias phases.

Classic exchange bias is thought to be driven by a 'hidden' disordered FM/AFM interface, where pinned uncompensated moments are localized and pinned by the antiferromagnetic phase[5]. Here, we remove the spectator ferromagnetic phase in a unique circumstance of intertwined spin-glass/antiferromagnetic phases. The present system does not rely on pinning at just a thin-film interface, but throughout the entire volume of the sample, essentially creating a macroscopic model interface. This provides critical insight into general exchange bias mechanisms; the cooperative action of spin-glass and antiferromagnetic order compromises the ergodic landscape of the spin glass, forcing the uncompensated moment to be pinned to one sublattice. Importantly, the coexistence of spin-glass and antiferromagnetic phases has been established in multiple systems[30–33], and their interplay may have a direct connection to systems in which disordered AFMs have been extensively studied in the context of the

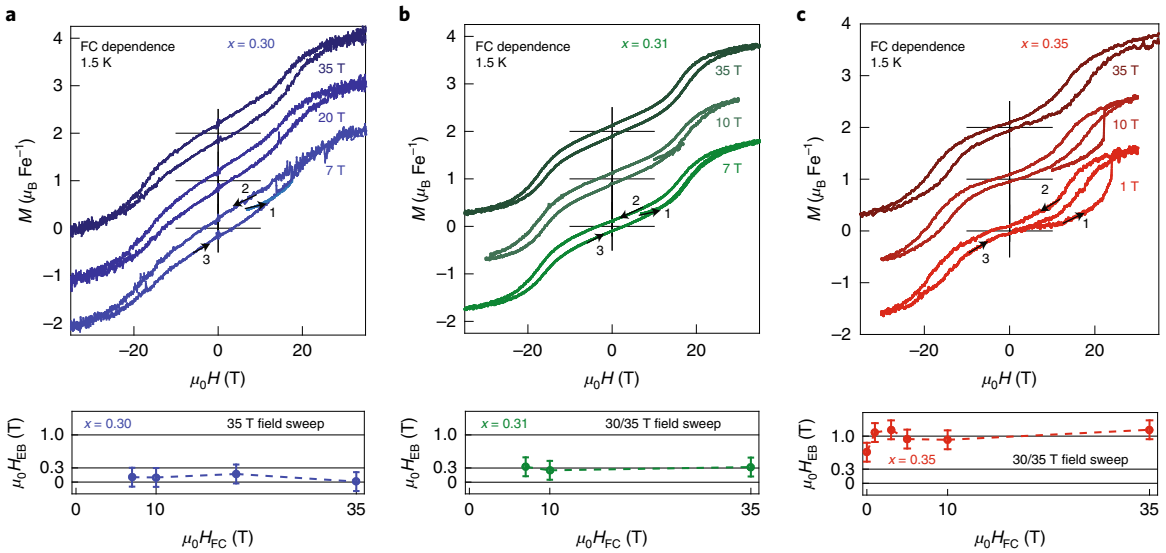

Fig. 5 | High-field exchange bias characterization. a–c, Out-of-plane magnetization versus high magnetic field sweeps (up to 35 T) measured after cooling in various magnetic fields from above the antiferromagnetic transition temperature down to 1.5 K. Each loop is offset on the *y* axis by $1\,\mu_B$ Fe^{-1}. The arrows and numbers present the sweep direction of the hysteresis loop for each intercalation. **a**, The $x = 0.30$ sample does not show any substantial exchange bias when swept up to 35 T in the range of the cooling fields taken (7–35 T). **b,** For the $x = 0.31$ sample, a stable exchange bias of approximately 0.3 T is captured in the same field range (7–35 T). **c**, The $x = 0.35$ sample shows a clear exchange bias of around 1 T at all implemented cooling fields (0–35 T), which demonstrates the high field sweep connection to the formation of exchange bias. Moreover, the metamagnetic transition clearly appears (in the initial field sweep direction) when the cooling field is weak enough, subsequently merging into the major hysteresis loop. The error bars are defined by the zero magnetization intercepts resolution.

random-field Ising model[34]. In this case, it is well established that random fields associated with disorder interact with the antiferromagnetic lattice, directly influencing the avalanche of domain flips in applied magnetic fields[35,36]. Random-field models of exchange bias in bilayer systems, which build upon these foundations, indeed afford results that hew closely to experimental exchange bias data[7,29,37]. In this light, the intimate coupling between an uncompensated spin glass and a highly anisotropic AFM within a single crystal unsurprisingly results in exchange bias that is orders of magnitude larger than in bilayer systems. In principle, this mechanism also pertains to bilayer systems, and suggests a material design strategy that incorporates anisotropy and magnetic disorder as a path to larger bias materials with broader technological application.

Online content

Any methods, additional references, Nature Research reporting summaries, source data, extended data, supplementary information, acknowledgements, peer review information; details of author contributions and competing interests; and statements of data and code availability are available at https://doi.org/10.1038/s41567-020-01123-w.

Received: 11 April 2019; Accepted: 11 November 2020;
Published online: 21 January 2021

References

1. Kools, J. Exchange-biased spin-valves for magnetic storage. *IEEE Trans. Magn.* **32**, 3165–3184 (1996).
2. He, X. et al. Robust isothermal electric control of exchange bias at room temperature. *Nat. Mater.* **9**, 579–585 (2010).
3. Meiklejohn, W. H. & Bean, C. P. New magnetic anisotropy. *Phys. Rev.* **102**, 1413–1414 (1956).
4. Ohldag, H. et al. Correlation between exchange bias and pinned interfacial spins. *Phys. Rev. Lett.* **91**, 017203 (2003).
5. Schuller, I. K., Morales, R., Batlle, X., Nowak, U. & Güntherodt, G. Role of the antiferromagnetic bulk spins in exchange bias. *J. Magn. Magn. Mater.* **416**, 2–9 (2016).
6. Kiwi, M. Exchange bias theory. *J. Magn. Magn. Mater.* **234**, 584–595 (2001).
7. Miltényi, P. et al. Diluted antiferromagnets in exchange bias: proof of the domain state model. *Phys. Rev. Lett.* **84**, 4224–4227 (2000).
8. Ali, M. et al. Exchange bias using a spin glass. *Nat. Mater.* **6**, 70–75 (2007).
9. Giri, S., Patra, M. & Majumdar, S. Exchange bias effect in alloys and compounds. *J. Phys. Condens. Matter* **23**, 073201 (2011).
10. Barnsley, L. C., Gray, E. M. & Webb, C. J. Asymmetric reversal in aged high concentration CuMn alloy. *J. Phys. Condens. Matter* **25**, 086003 (2013).
11. Hudl, M., Mathieu, R. & Nordblad, P. Tunable exchange bias in dilute magnetic alloys—chiral spin glasses. *Sci. Rep.* **6**, 19964 (2016).
12. Fischer, K. H. & Hertz, J. A. *Spin Glasses* (Cambridge Studies in Magnetism Vol. 1, Cambridge Univ. Press, 1993).
13. Mydosh, J. A. *Spin Glasses: An Experimental Introduction* (CRC Press, 2013).
14. Nagata, S., Keesom, P. H. & Harrison, H. R. Low-dc-field susceptibility of CuMn spin glass. *Phys. Rev. B* **19**, 1633–1638 (1979).
15. Binder, K. & Young, A. P. Spin glasses: experimental facts, theoretical concepts, and open questions. *Rev. Mod. Phys.* **58**, 801–976 (1986).
16. Dekker, C., Arts, A. F., de Wijn, H. W., van Duyneveldt, A. J. & Mydosh, J. A. Activated dynamics in a two-dimensional Ising spin glass: $Rb_2Cu_{1-x}Co_xF_4$. *Phys. Rev. B* **40**, 11243–11251 (1989).
17. Parisi, G. Order parameter for spin glasses. *Phys. Rev. Lett.* **50**, 1946–1948 (1983).
18. Van Laar, B., Rietveld, H. M. & Ijdo, D. J. W. Magnetic and crystallographic structures of Me_xNbS_2 and Me_xTaS_2. *J. Solid State Chem.* **3**, 154–160 (1971).
19. Suzuki, T., Ikeda, S., Richardson, J. W. & Yamaguchi, Y. Magnetic structure of $Fe_{1/3}NbS_2$. In *Proc. 5th International Symposium on Advanced Nuclear Energy Research* 343–346 (Japan Atomic Energy Research Institute, 1993).
20. Haley, S. C. et al. Half-magnetization plateau and the origin of threefold symmetry breaking in an electrically switchable triangular antiferromagnet. *Phys. Rev. Res.* **2**, 043020 (2020).
21. Doi, N. & Tazuke, Y. Spin glass phases in 2H-Fe_xNbS_2. *J. Phys. Soc. Jpn* **60**, 3980–3981 (1991).
22. Yamamura, Y. et al. Heat capacity and phase transition of Fe_xNbS_2 at low temperature. *J. Alloys Compd.* **383**, 338–341 (2004).
23. Tsuji, T., Yamamura, Y., Watanabe, H., Saito, K. & Sorai, M. Heat capacity of intercalated layered materials Fe_xNbS_2 at low temperature. *J. Therm. Anal. Calorim.* **57**, 839–846 (1999).
24. Parkin, S. S. P. & Friend, R. H. 3*d* transition-metal intercalates of the niobium and tantalum dichalcogenides. II. Transport properties. *Phil. Mag. B* **41**, 95–112 (1980).

25. Friend, R. H., Beal, A. R. & Yoffe, A. D. Electrical and magnetic properties of some first row transition metal intercalates of niobium disulphide. *Phil. Mag.* **35**, 1269–1287 (1977).
26. Little, A. et al. Three-state nematicity in the triangular lattice antiferromagnet $Fe_{1/3}NbS_2$. *Nat. Mater.* **19**, 1062–1067 (2020).
27. Nogués, J. & Schuller, I. K. Exchange bias. *J. Magn. Magn. Mater.* **192**, 203–232 (1999).
28. Büttgen, N., Kuhns, P., Prokofiev, A., Reyes, A. P. & Svistov, L. E. High-field NMR of the quasi-one-dimensional antiferromagnet $LiCuVO_4$. *Phys. Rev. B* **85**, 214421 (2012).
29. Malozemoff, A. Random-field model of exchange anisotropy at rough ferromagnetic-antiferromagnetic interfaces. *Phys. Rev. B* **35**, 3679–3682 (1987).
30. Wong, P. et al. Coexistence of spin-glass and antiferromagnetic orders in the Ising system $Fe_{0.55}Mg_{0.45}Cl_2$. *Phys. Rev. Lett.* **55**, 2043–2046 (1985).
31. Chillal, S. et al. Microscopic coexistence of antiferromagnetic and spin-glass states. *Phys. Rev. B* **87**, 220403 (2013).
32. Kleemann, W., Shvartsman, V. V., Borisov, P. & Kania, A. Coexistence of antiferromagnetic and spin cluster glass order in the magnetoelectric relaxor multiferroic $PbFe_{0.5}Nb_{0.5}O_3$. *Phys. Rev. Lett.* **105**, 257202 (2010).
33. Fu, Z. et al. Coexistence of magnetic order and spin-glass-like phase in the pyrochlore antiferromagnet $Na_3Co(Co_3)_2Cl$. *Phys. Rev. B* **87**, 214406 (2013).
34. Young, A. P. (ed.) *Spin Glasses and Random Fields* (Directions in Condensed Matter Physics Vol. 12, World Scientific, 1998).
35. Fishman, S. & Aharony, A. Random field effects in disordered anisotropic antiferromagnets. *J. Phys. C* **12**, L729 (1979).
36. Cardy, J. L. Random-field effects in site-disordered Ising antiferromagnets. *Phys. Rev. B* **29**, 505–507 (1984).
37. Malozemoff, A. P. Mechanisms of exchange anisotropy. *J. Appl. Phys.* **63**, 3874–3879 (1988).

Methods

Single crystals of Fe_xNbS_2 were synthesized by using a chemical vapour transport technique. A polycrystalline precursor was prepared from iron, niobium and sulfur in the ratio x:1:2 (Fe:Nb:S). The resulting polycrystalline product was then placed in an evacuated quartz ampoule with iodine as a transport agent (2.2 mg cm^{-3}), and put in the hot end of a two-zone MTI furnace with temperature set points of 800 °C and 950 °C for a period of seven days. High-quality hexagonal crystals with diameters of several millimetres were obtained. Low-field magnetization measurements were performed by using a Quantum Design MPMS-3 system with a maximum applied magnetic field of 7 T. High-field magnetization measurements were performed at the National High Magnetic Field Laboratory (NHMFL) by using a vibrating sample magnetometry system with a maximum applied magnetic field of 35 T. NMR measurements were performed by using the spin-echo technique at the Condensed Matter NMR laboratory at NHMFL by using a home-built NMR spectrometer with quadrature detection. Measurements were conducted by using the Hahn pulse sequence. The NMR signal was calculated by summing the area below the echo peak. The magnetic field was varied between 6 T and 10 T at various temperatures from 4.2 K to 100 K. The magnet was calibrated by using a standard current–field calibration curve, which is routinely checked with a calibrated sample. Heat capacity was measured by using an Xensor a.c. sensor in a cryogen-free magnet system. Powder X-ray diffraction measurements were performed by using a Rigaku Ultima IV system with a Cu Kα radiation. Energy-dispersive X-ray spectroscopy was performed with an Oxford Instruments X-MaxN 50 mm^2 system. Laue microdiffraction patterns were obtained using broadband X-rays from the Advanced Light Source focused to a 1 μm spot. To perform inductively coupled plasma optical emission spectroscopy, the samples were first digested in hot 65% nitric acid and then treated with an excess of hydrofluoric acid to ensure complete dissolution of niobium, and the solutions were subsequently diluted to appropriate concentrations. A Perkin Elmer Optima 7000 DV ICP-OES was used to perform inductively coupled plasma optical emission spectroscopy.

Data availability

Source data are provided with this paper. All other data that support the plots within this paper and other findings of this study are available from the corresponding authors upon reasonable request.

Acknowledgements

This work was supported as part of the Center for Novel Pathways to Quantum Coherence in Materials, an Energy Frontier Research Center funded by the United States Department of Energy, Office of Science, Basic Energy Sciences. Work by J.G.A. was partially supported by the EPiQS Initiative of the Gordon and Betty Moore Foundation through grant no. GBMF9067. R.A.M. and J.R.L. were supported by the National Science Foundation through award no. DMR-1611525. A portion of this work was performed at the National High Magnetic Field Laboratory, which is supported by the National Science Foundation cooperative agreement no. DMR-1644779 and the State of Florida. Laue microdiffraction measurements were done with the assistance of C. Stan in the Advanced Light Source beamline 12.3.2, which is an Office of Science User Facility of the Department of Energy, under contract no. DE-AC02-05CH11231.

Author contributions

E.M., S.D., C.J. and S.C.H. performed crystal synthesis and magnetization measurements. E.M. performed heat capacity, energy-dispersive X-ray spectroscopy and Laue microdiffraction measurements. R.A.M. and J.R.L. assisted in initial measurements and interpretation of glassy behaviour and exchange bias, and performed inductively coupled plasma analysis. A.M., S.K.R. and A.P.R. performed NMR measurements. Y.-L.T., P.E. and R.R. performed transmission electron microscopy measurements and analysis. E.M., R.A.M. and J.G.A. performed data analysis and wrote the manuscript with input from all co-authors.

Competing interests

The authors declare no competing interests.

Additional information

Supplementary information is available for this paper at https://doi.org/10.1038/s41567-020-01123-w.

Correspondence and requests for materials should be addressed to E.M. or J.G.A.

Peer review information *Nature Physics* thanks Per Nordblad and the other, anonymous, reviewer(s) for their contribution to the peer review of this work.

Reprints and permissions information is available at www.nature.com/reprints.